analytical chemistry

pubs.acs.org/ac Article

Ultrasensitive Nucleic Acid Assay Based on Cyclometalated Iridium(III) Complex with High Electrochemiluminescence Efficiency

Zhi-Hong Xu,‖ Hang Gao,‖ Nan Zhang, Wei Zhao,* Yi-Xiang Cheng, Jing-Juan Xu,* and Hong-Yuan Chen

Cite This: *Anal. Chem.* 2021, 93, 1686−1692 Read Online

ACCESS | Metrics & More | Article Recommendations | Supporting Information

ABSTRACT: This work developed a sensitive electrochemiluminescence (ECL) biosensor based on a cyclometalated iridium(III) complex ($(bt)_2Irbza$), which was synthesized for the first time. Annihilation, reductive−oxidative, and oxidative−reductive ECL behaviors of $(bt)_2Irbza$ were investigated, respectively. The oxidative−reductive ECL intensity was the strongest compared with the other two, which showed 16.7 times relative ECL efficiency compared with commercial $[Ru(bpy)_3]^{2+}$ under the same experimental conditions. Therefore, an ECL biosensing system with $(bt)_2Irbza$ as the anodic luminophore was established for miRNA detection based on a closed bipolar electrode (BPE). Combined with both steric hindrance and catalytic effects induced by hemin/G-quadruplex in the cathodic reservoir of BPE that changed the Faraday current of the cathode and thus mediated the ECL intensity of $(bt)_2Irbza$ in the anode of BPE, the ECL sensor stated an ultrahigh sensitivity for microRNA (miRNA-122) analysis with a detection limit of 82 aM.

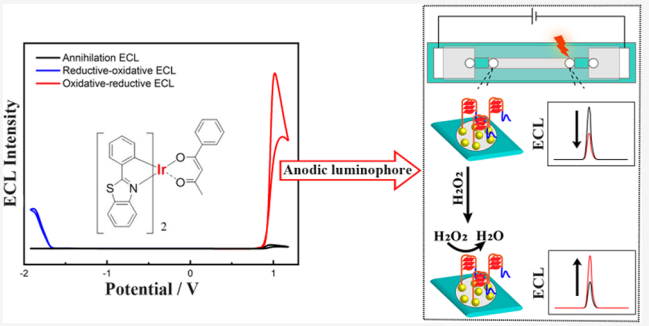

Electrochemiluminescence (ECL) is a light emission process of the luminophore introduced by electrochemical excitation,[1,2] which is widely used for bioanalysis due to its high sensitivity.[3−5] MicroRNAs (miRNAs) play an important role in several human diseases.[6] For example, the expression level of miRNA-21 is closely related to lung adenocarcinomas, breast cancer, etc.[7] As a new biomarker for liver injury, the analysis of miRNA-122 is conducive to the detection and monitoring of drug-induced liver injury.[8,9] Therefore, it is necessary to develop sensitive and efficient analytical strategies. To obtain better analytical performance, more and more studies were devoted to establish novel ECL systems, the development of which were mainly affected by coreactants, emitters, and electrodes.[10] ECL biosensing systems based on bipolar electrodes (BPEs) have been developed with promising potentials in clinical bioassays.[11−14] A BPE assembled in a microchannel with two poles in one solution was named as "open" BPE.[15] On the other hand, in a "closed" BPE system, two poles were separated in different reservoirs and different solutions could be used in this system.[15] Electrochemical processes occurred at the anodic and cathodic ends of the BPE when an external voltage was applied. In a "closed" BPE system, efforts were devoted to change the velocity of electron transfer in the sensing cell.[16,17] At the reporting cell, ECL signals were recorded to characterize the detection performance of the BPE system. Conventional ECL emitters, such as quantum dots and $Ru(bpy)_3^{2+}$, were generally used in the BPE−ECL system.[11,18] In recent years, novel materials with better ECL performance were synthesized, which offered a good opportunity for the BPE−ECL-based biosensor to enhance the sensing performances. Cyclometalated iridium(III) complexes, as one of the most promising ECL emitters, have been investigated in depth.[19] Due to their high ECL efficiency,[1] long luminescent lifetimes,[20] and excellent tunability with an emission range from 410 to 1180 nm via ligand changing,[21−23] cyclometalated iridium(III) complexes have been successfully applied in ECL systems for the detection of small biomolecules[24] and microRNAs,[25] as well as the construction of ECL devices including ECL gels[26] and multicolor ECL platform.[27] Kim's group[1] first reported two neutral cyclometalated iridium(III) complexes of $(pq)_2Ir(acac)$ and $(pq)_2Ir(tmd)$ with ECL efficiencies higher than $[Ru(bpy)_3]^{2+}$, (pq = 2-phenylquinoline anion, acac = acetylacetonate anion, tmd = 2,2′,6,6′-tetramethylhepta-3,5-dione anion).

Further, more researchers devoted their efforts to synthesize ECL materials of cyclometalated iridium(III) complexes with O∧O type ancillary ligands to achieve higher ECL

Received: October 12, 2020
Accepted: December 18, 2020
Published: December 30, 2020

https://dx.doi.org/10.1021/acs.analchem.0c04284
Anal. Chem. 2021, 93, 1686−1692

efficiency.[28−30] For example, Zhou's group[31] synthesized a number of iridium complexes with O∧O type ancillary ligands and different main ligands. Among them, 2-phenylbenzo[*d*]-thiazole (bt), as the main ligand, could significantly change the electron cloud distribution of iridium complexes, leading to lower triplet energy than that of the ancillary ligand, which benefited the ECL emission from the excited state of the $(C∧N)_2Ir$ fragment, eventually enhancing ECL efficiency.

Here, we synthesized a new cyclometalated iridium(III) complex, $(bt)_2Irbza$ (bza = 1-phenylbutane-1,3-dione anion), and explored its ECL mechanisms of annihilation, reductive−oxidative, and oxidative−reductive in detail. It was found that as an anodic luminophore, the relative ECL efficiency of $(bt)_2Irbza$ is 16.7 times that of $[Ru(bpy)_3]^{2+}$. Therefore, a biosensing system with $(bt)_2Irbza$ as the anodic ECL emitter of BPE was constructed for microRNA (miRNA) analysis (Scheme 1). In terms of the cathodic cell of BPE, hemin/G-quadruplex was generated based on the duplex-specific nuclease (DSN)-assisted simple target miRNA recycling strategy. Combined with the steric hindrance and catalytic effects caused by hemin/G-quadruplex, a sensitive biosensor for microRNA analysis with a detection limit of 82 aM was obtained.

Scheme 1. Schematic Representation of the Fabrication Process of the Closed BPE for miRNA-122 Detection

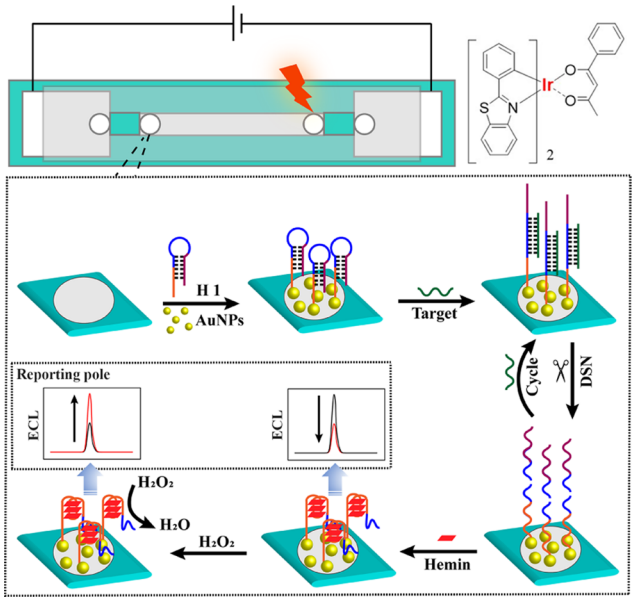

EXPERIMENTAL SECTION

Reagents and Apparatus. Reagents and Apparatus used in this work are exhibited in the Supporting Information (SI). DNA and miRNA sequences are presented in Table S1.

Synthesis of $(bt)_2Irbza$. The synthesis of iridium(III) complex is demonstrated in Scheme 2. A solution of $IrCl_3$ (1.0 g, 3.4 mmol) and 2-phenylbenzo[*d*]thiazole (1.44 g, 6.8 mmol) in a mixture of 2-ethoxyethanol/distilled water (15/5 mL) was refluxed at 120 °C under an argon atmosphere for 24 h. After the solution was cooled, the resulting mixture was filtered, and the precipitate was washed with water, ethanol, and *n*-hexane successively. After drying, the dichlorobridged iridium(III) dimer was obtained. The obtained dichlorobridged iridium-(III) dimer (300 mg, 0.23 mmol), benzoyl propanone (82.6 mg, 0.51 mmol), and Na_2CO_3 (538.6 mg, 5.1 mmol) in 2-ethoxyethanol (15 mL) were refluxed at 120 °C for 24 h. After the mixture was cooled to room temperature, the solvent was roto-evaporated. The residue was purified on a silica gel column with dichloromethane/methanol (50:1−15:1) to afford the $(bt)_2Irbza$ complex (red solid, yield: 61%).

Scheme 2. Synthesis of $(bt)_2Irbza$

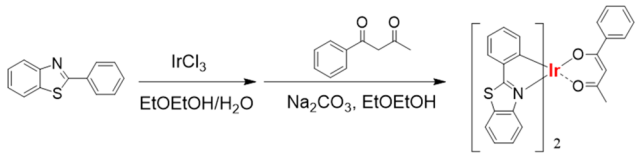

Electrochemical and ECL Measurements Using a Three-Electrode System. The electrochemical and ECL properties were detected by a three-electrode system, which includes a $Ag/AgNO_3$ (10 mM, acetonitrile) nonaqueous quasi-reference electrode, a platinum wire counter electrode, and a glassy carbon electrode (GCE, 3 mm in diameter). GCE was polished with alumina slurry, followed by ultrasonication in ultrapure water and ethanol in turn. Taking ferrocene (Fc) as an internal standard, the redox potential of ferrocene/ferrocenium (Fc/Fc^+) was tested with a saturated calomel electrode (SCE) as the reference electrode. The same experiment was conducted again with the $Ag/AgNO_3$ non-aqueous electrode as quasi-reference electrode. Thus, the quasi-reference electrode was calibrated against the SCE by comparing both redox potentials of ferrocene/ ferrocenium (Fc/Fc^+).

Preparation of the Closed BPE Biosensor. The fabrication of the closed BPE biosensor is exhibited in Scheme 1. 10 μL of 1.0×10^{-6} M H1 (the S−S bond was cut with 10 mM TCEP before use) was dropped into the cathodic cell of the closed BPE and allowed to react at 4 °C overnight. Then, the electrode was washed with 0.1 M PBS to get rid of the unbound H1. Subsequently, 100 μM MCH was used to block the unspecified active binding sites and urge the modified H1 to adopt an upright surface orientation for next hybridization. Afterward, different concentrations of target miRNA-122 were added to the cathodic cell of the closed BPE and incubated at 37 °C for 2 h. H1 was opened in the presence of miRNA-122, and the DNA−RNA heteroduplex was obtained. Next, excess DSN was added and incubated at 42.5 °C for 1.5 h to completely digest the DNA sequence in the DNA−RNA heteroduplex and recycle the target of miRNA-122. Finally, the electrodes were incubated with 0.2 mM hemin (20 mM HEPES, 50 mM KCl, 200 mM NaCl, 1% DMSO) at 37 °C for 1 h, leading to the generation of hemin/G-quadruplex.

ECL Detection Using the Closed BPE System. The cathodic poles were filled with 80 μL of 3 mM H_2O_2 for the ECL detection based on the catalytic effect, while 80 μL of 0.1 M PBS (pH 7.4) for the steric hindrance effect. The anodic reservoirs were both immersed in 80 μL of acetonitrile containing 0.1 M $TBAPF_6$, 0.1 mM $(bt)_2Irbza$, and 20 mM tripropylamine (TPrA). CHI-600E electrochemical workstation was used to apply a linear sweep voltammetry scan from 0 to 6.5 V.

RESULTS AND DISCUSSION

Characterization of $(bt)_2Irbza$. A cyclometalated iridium-(III) complex ($(bt)_2Irbza$) with high ECL efficiency was synthesized and employed as an ECL luminophore at the

https://dx.doi.org/10.1021/acs.analchem.0c04284
Anal. Chem. 2021, 93, 1686−1692

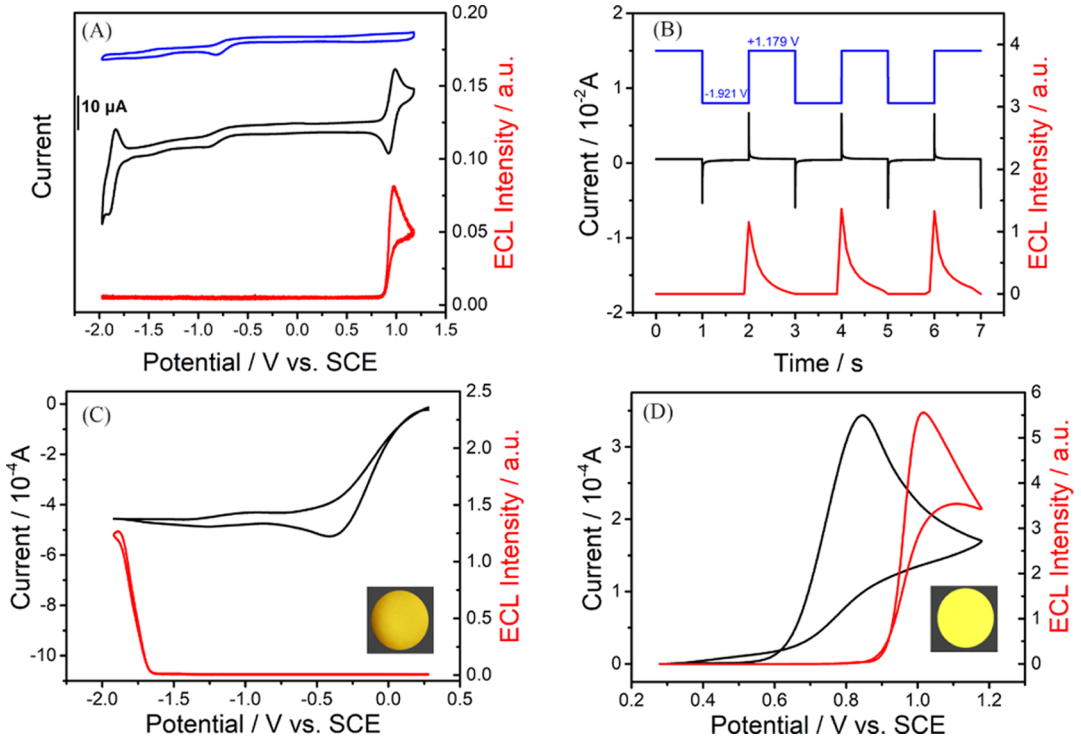

Figure 1. (A) CV curves without (blue line) and with (black line) $(bt)_2Irbza$ as well as annihilation ECL intensity−potential curve of 0.1 mM $(bt)_2Irbza$ in CH_3CN containing 0.1 M $TBAPF_6$ (voltage of PMT, 600 V). (B) Transient profiles of potential (blue), current (black), and ECL (red) of 0.1 mM $(bt)_2Irbza$ in CH_3CN containing 0.1 M $TBAPF_6$ (voltage of PMT, 600 V). (C) Cyclic voltammetry curve (black line) and ECL profile (red line) of 0.1 mM $(bt)_2Irbza$ containing 20 mM BPO (voltage of PMT, 300 V). (D) Cyclic voltammetry curve (black line) and ECL profile (red line) of 0.1 mM $(bt)_2Irbza$ containing 20 mM TPrA (voltage of PMT, 300 V).

anodic pole of BPE. Figures S1 and S2 in the Supporting Information show the ^1H NMR and ^{13}C NMR spectra of $(bt)_2Irbza$ and provide the corresponding nuclear magnetic peaks. Mass spectrum is displayed in Figure S3, which further confirmed the successful synthesis of $(bt)_2Irbza$. In addition, $(bt)_2Irbza$ possesses a relatively long PL lifetime with 0.92 μs (Figure S4) compared to other iridium(III) complexes,[32] which was beneficial to the radiative decay rates, thus prompting the PL emission.[33] Besides, UV−vis absorption was also measured and exhibited in Figure S5. The result proved the existence of metal-to-ligand charge transfer transitions (MLCT) of $(bt)_2Irbza$ with the well-resolved weak absorptions from 420 to 580 nm.

Cyclic voltammetry (CV) was used to explore the electrochemical property of $(bt)_2Irbza$, which was dissolved in CH_3CN containing 0.1 M $TBAPF_6$. As shown in Figure 1A (black line), a reversible redox process with the formal potential of 0.957 V vs SCE, corresponding to the single electron redox reaction of iridium complex, was observed. On the other hand, the quasi-reversible redox signal was also noticed with the formal potential of −1.872 V vs SCE, which might be attributed to the redox process of the ancillary ligand[34] and was proved by the control experiment without addition of $(bt)_2Irbza$ (blue line).

To investigate the ECL performance of $(bt)_2Irbza$, annihilation ECL was first tested. The ECL of 0.1 mM $(bt)_2Irbza$ without a coreactant was cyclically scanned from −1.921 to 1.179 V vs SCE. The possible ECL mechanism shows as follows[35,36]

$$[(bt)_2Irbza] + e^- \rightarrow [(bt)_2Irbza]^{\bullet -} \quad (1)$$

$$[(bt)_2Irbza] - e^- \rightarrow [(bt)_2Irbza]^{\bullet +} \quad (2)$$

$$[(bt)_2Irbza]^{\bullet -} + [(bt)_2Irbza]^{\bullet +} \rightarrow [(bt)_2Irbza]^* \quad (3)$$

$$[(bt)_2Irbza]^* \rightarrow [(bt)_2Irbza] + h\nu \quad (4)$$

As displayed in Figure 1A (red line), the annihilation ECL signal at positive potential was stronger than that at negative potential, with negative scanning from 0 to −1.921 V and then positive scanning to 1.179 V. Moreover, the transient ECL profile was investigated by a potential step pulse between −1.921 and 1.179 V vs SCE with a pulse width of 1 s. The current and ECL signals are displayed in Figure 1B. ECL signal was hardly observed after the potential switched from 1.179 to −1.921 V. However, a significant ECL signal appeared on the reversal step, indicating that the anionic radical anion ($[(bt)_2Irbza]^{\bullet -}$) was more stable than the cationic radical anion ($[(bt)_2Irbza]^{\bullet +}$).

Subsequently, reductive−oxidative and oxidative−reductive ECL performances in the presence of coreactants were studied, respectively. Reductive−oxidative ECL of 0.1 mM $(bt)_2Irbza$ with 20 mM benzoyl peroxide (BPO) is shown in Figure 1C. The concentration of the coreactant was optimized (Figure S6). The irreversible reductive signal with a peak potential of −0.363 V vs SCE observed in Figure 1C (black line) was corresponded to BPO, which was consistent with the CV curve of BPO in Figure S7. Obvious ECL signal was observed in Figure 1C (red line). During the negative potential scanning, the highest ECL signal (1.268 a.u.) was obtained with an onset potential of −1.635 V, which was close to the reduction of $(bt)_2Irbza$ with an onset potential of −1.624 V in Figure 1A (black line). Based on previous reports of iridium(III)

https://dx.doi.org/10.1021/acs.analchem.0c04284
Anal. Chem. 2021, 93, 1686−1692

complexes/BPO systems,[37,38] the ECL mechanism of $(bt)_2$Irbza/BPO is as follows

$$BPO + e^- \rightarrow BPO^{\bullet -} \quad (5)$$

$$BPO^{\bullet -} \rightarrow C_6H_5CO_2^- + C_6H_5CO_2^{\bullet} \quad (6)$$

$$[(bt)_2Irbza] + e^- \rightarrow [(bt)_2Irbza]^{\bullet -} \quad (7)$$

$$[(bt)_2Irbza]^{\bullet -} + C_6H_5CO_2^{\bullet} \rightarrow [(bt)_2Irbza]^* + C_6H_5CO_2^- \quad (8)$$

$$[(bt)_2Irbza]^* \rightarrow [(bt)_2Irbza] + h\nu \quad (9)$$

Further, oxidative−reductive ECL of 0.1 mM $(bt)_2$Irbza was explored with an optimized concentration (20 mM) of TPrA (Figure S8). As revealed in Figure 1D (black line), an irreversible oxidation peak of TPrA was observed, and the redox peaks of $(bt)_2$Irbza were not obvious in this system. ECL response (5.557 a.u.) was observed with an onset potential of 0.860 V (red line), which was close to the onset potential of 0.830 V of the oxidation of $(bt)_2$Irbza (Figure 1A, black line). In addition, compared with annihilation and reductive−oxidative ECL, the oxidative−reductive ECL showed the most significant response. Based on previous studies,[34,39−41] the possible ECL mechanism of $(bt)_2$Irbza/TPrA is shown as follows

$$TPrA \rightarrow TPrA^{\bullet +} + e^- \quad (10)$$

$$TPrA^{\bullet +} \rightarrow TPrA^{\bullet} + H^+ \quad (11)$$

$$[(bt)_2Irbza] - e^- \rightarrow [(bt)_2Irbza]^{\bullet +} \quad (12)$$

$$[(bt)_2Irbza]^{\bullet +} + TPrA^{\bullet} \rightarrow [(bt)_2Irbza]^* + \text{product} \quad (13)$$

$$[(bt)_2Irbza]^* \rightarrow [(bt)_2Irbza] + h\nu \quad (14)$$

As mentioned above, the anion radical was more stable than the cationic radical, however, the oxidative−reductive ECL with TPrA as the coreactant was higher than the reductive−oxidative ECL with BPO as the coreactant. A possible reason is that close potential for the formation of TPrA radical and $[(bt)_2Irbza]^{\bullet +}$, resulting in higher ECL intensity.[42] Additional studies were conducted to further explore the oxidative−reductive ECL property of $(bt)_2$Irbza. ECL relative efficiency was quantified as[21,43]

$$\varnothing_x = \varnothing_{st}\left(\frac{\int_0^t I\,dt}{\int_0^t i\,dt}\right)_x \Big/ \left(\frac{\int_0^t I\,dt}{\int_0^t i\,dt}\right)_{st} \quad (15)$$

$\varnothing_{st}$ represents the ECL efficiency of 0.1 mM $[Ru(bpy)_3]^{2+}$ when CH_3CN containing 0.1 M $TBAPF_6$ and 20 mM TPrA serves as the standard and the ECL efficiency is set as 1. *x*, st, *I*, and *i* act as the sample, $[Ru(bpy)_3]^{2+}$, ECL intensity, and current value, respectively. The value of $\varnothing_x$ is 16.7, indicating that $(bt)_2$Irbza shows 16.7 times relative ECL quantum efficiency than $[Ru(bpy)_3]^{2+}$. The oxidative−reductive ECL stability of $(bt)_2$Irbza was investigated and displayed in Figure S9. A good stability was obtained for the consecutive ECL scans of 10 cycles with a relative standard deviation of 2.6%. Furthermore, the ECL performance of $(bt)_2$Irbza as the anodic emitter on BPE was also tested. The ECL intensity increased gradually as the concentration of $(bt)_2$Irbza increased from 0.05 to 0.25 mM (Figure S10A). To reduce cost and environmental pollution, we chose a lower concentration of 0.1 mM $(bt)_2$Irbza, and the ECL strength at this concentration is sufficient compared to $[Ru(bpy)_3]^{2+}$ (Figure S10B) for the following nucleic acid detection.

The spectra of photoluminescence (PL) and ECL with different reaction mechanisms were further collected (Figure S11). The PL emission peak is centered at 560 nm, while the annihilation, the reductive−oxidative, and the oxidative−reductive ECL emission peaks are centered at 556, 563, and 562 nm, respectively, which are close to the PL emission. The experimental findings of the new iridium complex parameters are summarized in Table S2.

Detection Principle of the BPE−ECL Biosensor. An ECL−BPE sensor with $(bt)_2$Irbza was established for miRNA detection due to its great oxidative−reductive ECL property. Scheme 1 illustrates the fabrication of the ECL−BPE system. A thiol-group-terminated hairpin DNA 1 (H1) containing a recognition sequence for the target miRNA-122 (blue part) and G-quadruplex sequence (orange part) and the rest sequence (purple part) was assembled on the Au nanoparticle (AuNP)-modified cathode of the closed BPE via a Au−S bond. DSN was then introduced to cleave the hairpin DNA 1 complementary to miRNA-122 in DNA−miRNA heteroduplex and release the target miRNA. Recycling of miRNA-122 led to the continuous opening of the hairpin DNA 1 and the generation of "active" G-quadruplex structures. At last, after being incubated with hemin, the liberated G-quadruplexes were folded into a supramolecular hemin/G-quadruplex. To confirm the feasibility of the target recycling strategy, the polyacrylamide gel electrophoresis (PAGE) analysis was applied in this work. The result is shown in Figure 2. Lanes

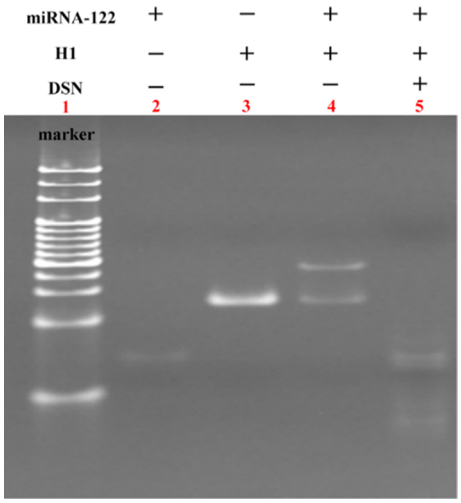

Figure 2. Characterization of different structures using PAGE. Lanes: (1) marker, (2) miRNA-122, (3) H1, (4) mixture of miRNA-122 and H1, and (5) mixture of miRNA-122, H1, and DSN.

2 and 3 represent the gel electrophoresis of miRNA-122 and H1 alone. Lane 4 verifies the hybridization of miRNA-122 and H1. The addition of DSN resulted in the cleavage of DNA sequence in the H1/miRNA structure and the release of the target miRNA-122.

At the sensing pole, the assembly of hemin/G-quadruplex would limit the electron transfer due to its own steric hindrance, leading to the suppression of ECL at the anode. However, H_2O_2 was catalyzed by hemin/G-quadruplex

https://dx.doi.org/10.1021/acs.analchem.0c04284
Anal. Chem. 2021, 93, 1686−1692

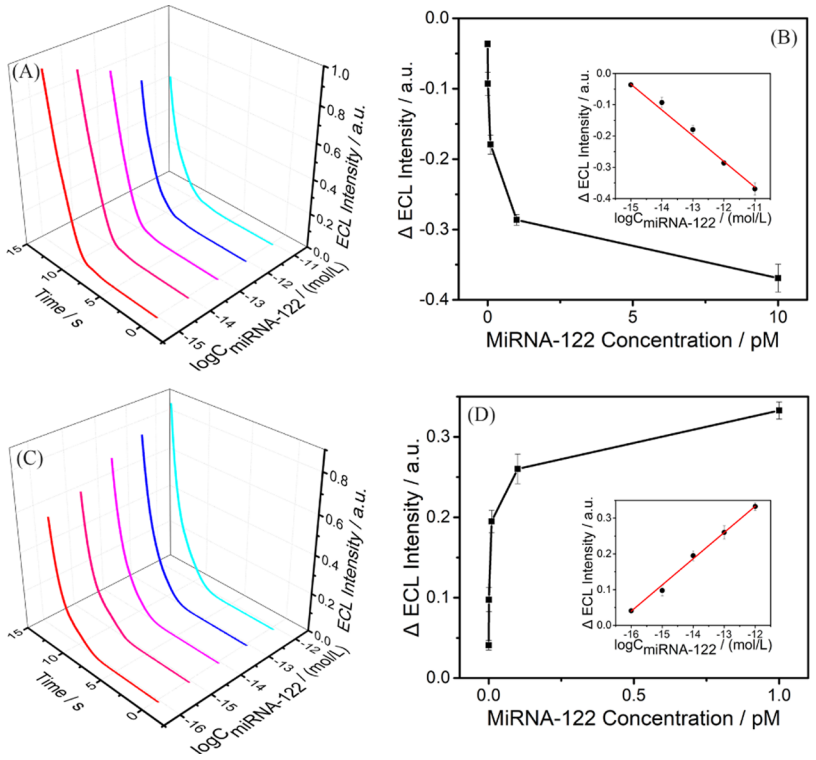

Figure 3. (A) ECL profiles of the BPE−ECL biosensor incubated with different concentrations of miRNA-122 ranging from 10^{-15} to 10^{-11} M (voltage of PMT, 600 V). (B) ECL signal changes in the presence of different concentrations of miRNA-122 (from left to right, 1 fM, 10 fM, 0.1 pM, 1 pM, and 10 pM) (voltage of PMT, 600 V). Inset: the linear relationship. (C) ECL signals of the BPE−ECL sensor for miRNA-122 with different concentrations ranging from 10^{-16} to 10^{-12} M (voltage of PMT, 500 V). (D) Relationship between ΔECL and the concentrations of miRNA-122 (from left to right, 100 aM, 1 fM, 10 fM, 0.1 pM, and 1 pM) (voltage of PMT, 500 V). Inset: the linear relationship. Error bars represented the standard deviations for each set of three parallel experiments.

DNAzyme[44,45] when 0.1 M PBS was replaced by 0.1 M PBS containing 3 mM H_2O_2 in the cathodic cell, followed by enhancing the Faraday current of the cathode. To maintain the charge balance within the BPE, the oxidation of $(bt)_2$Irbza and TPrA was accelerated and then the ECL intensity was increased. The miRNA analysis from different detection methods was integrated into a single sensor interface. Moreover, both strategies were easy to be operated, and different dynamic concentration ranges and detection sensitivities could be obtained on the basis of different sensing strategies.

ECL Analysis of miRNA-122. As illustrated in Figure 3A, the ECL intensity decreased with the increasing concentration of miRNA-122. Figure 3B shows the relationship between the ΔECL (the ECL difference between the stage of H1 modification and the stage of hemin/G-quadruplex assembly) and the concentration of target miRNA-122. It was found that both were in linear correlation between the ECL intensity and the logarithm of target concentration in the range from 10^{-15} to 10^{-11} M with the linear fitting equation $\Delta ECL = -1.269 - 0.082 \times \lg C$ ($R^2 = 0.993$) (Figure 3B, inset). To improve the limit of detection (LOD), H_2O_2 was added into the cathodic reservoir. As Figure 3C exhibits, the ECL signal enhanced when the concentration of miRNA-122 changed from 10^{-16} to 10^{-12} M, which declared that the catalytic effect was dominant during the process although the steric hindrance effect also existed. Figure 3D shows the relationship between ΔECL and different miRNA-122 concentrations. A good linear relationship was obtained in the range 10^{-16}−10^{-12} M, and the fitting equation was $\Delta ECL = 1.214 + 0.073 \times \lg C$ ($R^2 = 0.997$) (Figure 3D, inset). LOD was calculated to be 82 aM. The results proved that higher sensitivity can be obtained based on the catalytic reduction of H_2O_2 by hemin/G-quadruplex DNAzyme. The LOD was also far lower than the previous reports on miRNA detection (Table S3).

Specificity and Sample Analysis. The specificity was evaluated by comparing the different ECL responses for miRNA-122, single-base mismatched miRNA sequence, miRNA-21, and miRNA-141 with the same concentration. Meanwhile, blank was applied as a reference. As shown in Figure S12, miRNA-21, miRNA-141, and blank showed little difference in ECL intensity and evidently lower than miRNA-122. The ECL intensity for single-base mismatched miRNA sequence was slightly increased but still obviously lower than that of target miRNA-122. The result illustrates that the ECL signal was enhanced evidently only in the presence of target miRNA-122, showing an acceptable specificity of the BPE−ECL biosensor.

To test the feasibility of the BPE−ECL biosensing system, we employed standard addition of miRNA-122 in 10% diluted normal fetal calf serum to test the practical application. Based on the steric hindrance effect, the sensor exhibited good practical application with recoveries from 97 to 106% and relative standard deviations (RSDs) from 1.7 to 3.5% for determination of miRNA-122 (Table 1). Based on the catalytic effect, good performance with recoveries from 91 to 104% and relative standard deviations (RSDs) from 1.8 to 2.9% for determination of miRNA-122 was achieved (Table 2). In general, the results illustrated that the proposed sensor attained satisfactory practical analysis of miRNA-122.

https://dx.doi.org/10.1021/acs.analchem.0c04284
Anal. Chem. 2021, 93, 1686−1692

Table 1. Recovery Tests for miRNA-122 in Spiked Fetal Calf Serum Samples (n = 3) (Based on the Steric Hindrance Effect)

samples	added	found	RSD (%)	recovery (%)
1	1.0 fM	1.01 fM	1.7	101
2	10.0 fM	10.6 fM	2.5	106
3	100 fM	106 fM	2.9	106
4	1.0 pM	0.97 pM	1.8	97
5	10.0 pM	9.8 pM	3.5	98

Table 2. Recovery Tests for miRNA-122 in Spiked Fetal Calf Serum Samples (n = 3) (Based on the Catalytic Effect)

samples	added	found	RSD (%)	recovery (%)
1	100 aM	98 aM	1.8	98
2	1.0 fM	1.03 fM	1.9	103
3	10.0 fM	10.4 fM	2.0	104
4	100 fM	92 fM	2.7	91
5	1.0 pM	0.93 pM	2.9	92

CONCLUSIONS

In conclusion, we synthesized a new cyclometalated iridium(III) complex ($(bt)_2$Irbza) for the first time and explored three luminescence mechanisms, including annihilation, reductive–oxidative, and oxidative–reductive ECL. The signal of oxidative–reductive ECL was the highest by comparing the performance of ECL. As a novel ECL emitter, $(bt)_2$Irbza exhibits excellent efficiency. The relative ECL quantum efficiency of the $(bt)_2$Irbza/TPrA system was 16.7 times compared to that of the $[Ru(bpy)_3]^{2+}$/TPrA pair. This shows a promising potential to design a reliable ECL sensor. In this work, an ECL–BPE sensor was constructed for miRNA analysis due to the superiority of oxidative–reductive ECL. Combining two sensing modes based on the steric hindrance and catalytic reduction, different linear ranges and limits of detection were obtained, with LOD calculated to be 82 aM. The proposed BPE–ECL sensor on the basis of highly efficient iridium complex showed good application perspective in the clinic analysis.

ASSOCIATED CONTENT

Supporting Information

The Supporting Information is available free of charge at https://pubs.acs.org/doi/10.1021/acs.analchem.0c04284.

Reagents; apparatus; design and fabrication of closed BPE; ^{1}H NMR spectra of $(bt)_2$Irbza; ^{13}C NMR spectra of $(bt)_2$Irbza; mass spectra of $(bt)_2$Irbza; phosphorescent lifetime of $(bt)_2$Irbza; UV–vis absorption and fluorescence spectra of $(bt)_2$Irbza; optimization of the concentration of BPO; cyclic voltammetry characterization of BPO; optimization of the concentration of TPrA; the ECL stability; optimization of the concentration of $(bt)_2$Irbza and ECL intensity comparation; the spectra of photoluminescence and ECL; summarization of the experimental findings for $(bt)_2$Irbza; comparison of the BPE–ECL biosensor and previous reports on miRNA detection; and specificity. (PDF)

AUTHOR INFORMATION

Corresponding Authors

Wei Zhao − *State Key Laboratory of Analytical Chemistry for Life Science, School of Chemistry and Chemical Engineering, Nanjing University, Nanjing 210023, China;* orcid.org/0000-0002-9526-2008; Email: weizhao@nju.edu.cn

Jing-Juan Xu − *State Key Laboratory of Analytical Chemistry for Life Science, School of Chemistry and Chemical Engineering, Nanjing University, Nanjing 210023, China; College of Chemistry and Molecular Engineering, Zhengzhou University, Zhengzhou 450001, China;* orcid.org/0000-0001-9579-9318; Phone: +86-25-89687924; Email: xujj@nju.edu.cn

Authors

Zhi-Hong Xu − *State Key Laboratory of Analytical Chemistry for Life Science, School of Chemistry and Chemical Engineering, Nanjing University, Nanjing 210023, China*

Hang Gao − *Key Lab of Mesoscopic Chemistry of MOE and Jiangsu Key Laboratory of Advanced Organic Materials, School of Chemistry and Chemical Engineering, Nanjing University, Nanjing 210023, China*

Nan Zhang − *State Key Laboratory of Analytical Chemistry for Life Science, School of Chemistry and Chemical Engineering, Nanjing University, Nanjing 210023, China*

Yi-Xiang Cheng − *Key Lab of Mesoscopic Chemistry of MOE and Jiangsu Key Laboratory of Advanced Organic Materials, School of Chemistry and Chemical Engineering, Nanjing University, Nanjing 210023, China;* orcid.org/0000-0001-6992-4437

Hong-Yuan Chen − *State Key Laboratory of Analytical Chemistry for Life Science, School of Chemistry and Chemical Engineering, Nanjing University, Nanjing 210023, China*

Complete contact information is available at: https://pubs.acs.org/10.1021/acs.analchem.0c04284

Author Contributions

‖Z.-H.X. and H.G. contributed equally. The manuscript was written through contributions of all authors. All authors have given approval to the final version of the manuscript.

Notes

The authors declare no competing financial interest.

ACKNOWLEDGMENTS

We gratefully acknowledge the National Key R&D Program of China (Grant 2016YFA0201200), the National Natural Science Foundation of China (Grants No. 22034003), and the Excellent Research Program of Nanjing University (ZYJH004).

REFERENCES

(1) Kim, A. J.; Shin, I. S.; Kim, H.; Lee, J. K. *J. Am. Chem. Soc.* **2005**, *127*, 1614–1615.

(2) Zanarini, S.; Rampazzo, E.; Ciana, L. D.; Marcaccio, M.; Marzocchi, E.; Montalti, M.; Paolucci, F.; Prodi, L. *J. Am. Chem. Soc.* **2009**, *131*, 2260–2267.

(3) Ni, J. C.; Lin, H.; Yang, W. Q.; Liao, Y. H.; Wang, Q. X.; Luo, F.; Guo, L. H.; Qiu, B.; Lin, Z. Y. *Anal. Chem.* **2019**, *91*, 14751–14756.

(4) Sun, Y. D.; Wang, Q. W.; Mi, L.; Shi, L.; Li, T. *Anal. Chem.* **2019**, *91*, 12948–12953.

(5) Han, Z. L.; Shu, J. N.; Liang, X.; Cui, H. *Anal. Chem.* **2019**, *91*, 12260–12267.

(6) Shi, C. X.; Li, S. X.; Chen, Z. P.; Liu, Q.; Yu, R. Q. *Anal. Chem.* **2019**, *91*, 2120−2127.
(7) Miyagawa, A.; Harada, M.; Okada, T. *Anal. Chem.* **2018**, *90*, 13729−13735.
(8) Leelahavanichkul, A.; Somparn, P.; Panich, T.; Chancharoenthana, W.; Wongphom, J.; Pisitkun, T.; Hirankarn, N.; Eiam-Ong, S. *Hepatol. Res.* **2015**, *45*, 1341−1352.
(9) Šípová, H.; Zhang, S.; Dudley, A. M.; Galas, D.; Wang, K.; Homola, J. *Anal. Chem.* **2010**, *82*, 10110−10115.
(10) Ma, C.; Cao, Y.; Gou, X.; Zhu, J. J. *Anal. Chem.* **2020**, *92*, 431−454.
(11) Lu, H. J.; Zhao, W.; Xu, J. J.; Chen, H. Y. *Biosens. Bioelectron.* **2018**, *102*, 624−630.
(12) Wang, Y. Z.; Ji, S. Y.; Xu, H. Y.; Zhao, W.; Xu, J. J.; Chen, H. Y. *Anal. Chem.* **2018**, *90*, 3570−3575.
(13) Wang, Y. Z.; Xu, C. H.; Zhao, W.; Guan, Q. Y.; Chen, H. Y.; Xu, J. J. *Anal. Chem.* **2017**, *89*, 2017−2023.
(14) Wang, Y. Z.; Zhao, W.; Dai, P. P.; Lu, H. J.; Xu, J. J.; Pan, J.; Chen, H. Y. *Biosens. Bioelectron.* **2016**, *86*, 683−689.
(15) Gross, E. M.; Anderson, J. D.; Slaterbeck, A. F.; Thayumanavan, S.; Barlow, S.; Zhang, Y.; Marder, H. K.; Hall, S. R.; Nabor, M. F.; Wang, J. F.; Mash, E. A.; Armstrong, N. R.; Wightman, R. M. *J. Am. Chem. Soc.* **2000**, *122*, 4972−4979.
(16) Cao, J. T.; Wang, Y. L.; Zhang, J. J.; Dong, Y. X.; Liu, F. R.; Ren, S. W.; Liu, Y. M. *Anal. Chem.* **2018**, *90*, 10334−10339.
(17) Wu, M. S.; Yuan, D. J.; Xu, J. J.; Chen, H. Y. *Anal. Chem.* **2013**, *85*, 11960−11965.
(18) Zhang, H. R.; Wang, Y. Z.; Zhao, W.; Xu, J. J.; Chen, H. Y. *Anal. Chem.* **2016**, *88*, 2884−2890.
(19) Liu, Z. Y.; Qi, Y. J.; Xu, G. B. *Chem. Soc. Rev.* **2015**, *44*, 3117−3142.
(20) Richter, M. M. *Chem. Rev.* **2004**, *104*, 3003−3036.
(21) Gao, H.; Zhang, N.; Li, Y.; Zhao, W.; Quan, Y.; Cheng, Y.; Chen, H. Y.; Xu, J. J. *Sci. China Chem.* **2020**, *63*, 715−721.
(22) Park, H. -Y.; Maheshwaran, A.; Moon, C. -K.; Lee, H.; Reddy, S. S.; Sree, V. G.; Yoon, J.; Kim, J. W.; Kwon, J. H.; Kim, J. -J.; Jin, S. -H. *Adv. Mater.* **2020**, *32*, No. 2002120.
(23) Liu, B.; Lystrom, L.; Cameron, C. G.; Kilina, S.; McFarland, S. A.; Sun, W. *Eur. J. Inorg. Chem.* **2019**, 2208−2215.
(24) Zhan, Z. X.; Su, Z. S.; Chai, L.; Li, C. G.; Liu, R.; Lv, Y. *Anal. Chem.* **2020**, *92*, 8285−8291.
(25) Gao, T. B.; Zhang, J. J.; Wen, J.; Yang, X. X.; Ma, H. B.; Cao, D. K.; Jiang, D. C. *Anal. Chem.* **2020**, *92*, 1268−1275.
(26) Moon, H. C.; Lodge, T. P.; Frisbie, C. D. *J. Am. Chem. Soc.* **2014**, *136*, 3705−3712.
(27) Voci, S.; Duwald, R.; Grass, S.; Hayne, D. J.; Bouffier, L.; Francis, P. S.; Lacour, J.; Sojic, N. *Chem. Sci.* **2020**, *11*, 4508−4515.
(28) Zdrachek, E.; Bakker, E. *Anal. Chem.* **2019**, *91*, 2−26.
(29) Trujano-Ortiz, L. G.; González, F. J.; Quintanar, L. *Inorg. Chem.* **2015**, *54*, 4−6.
(30) Zhou, Y.; Li, W.; Yu, L.; Liu, Y.; Wang, X.; Zhou, M. *Dalton Trans.* **2015**, *44*, 1858−1865.
(31) Zhou, Y.; Gao, H.; Wang, X.; Qi, H. *Inorg. Chem.* **2015**, *54*, 1446−1453.
(32) Kwon, T.-H.; Cho, H. S.; Kim, M. K.; Kim, J.-W.; Kim, J.-J.; Lee, K. H.; Park, S. J.; Shin, I.-S.; Kim, H.; Shin, D. M.; Chung, Y. K.; Hong, J.-I. *Organometallics* **2005**, *24*, 1578−1585.
(33) Chen, L.; Jiang, Y.; Nie, H.; Hu, R.; Kwok, H. S.; Huang, F.; Qin, A.; Zhao, Z.; Tang, B. Z. *ACS Appl. Mater. Interfaces* **2014**, *6*, 17215−17225.
(34) Shin, I.-S.; Kim, J. I.; Kwon, T.-H.; Hong, J.-I.; Lee, J.-K.; Kim, H. *J. Phys. Chem. C* **2007**, *111*, 2280−2286.
(35) Swanick, K. N.; Ladouceur, S.; Zysman-Colman, E.; Ding, Z. *Chem. Commun.* **2012**, *48*, 3179−3181.
(36) Kerr, E.; Doeven, E. H.; Barbante, G. J.; Hogan, C. F.; Hayne, D. J.; Donnelly, P. S.; Francis, P. S. *Chem. Sci.* **2016**, *7*, 5271−5279.
(37) Kesarkar, S.; Rampazzo, E.; Valenti, G.; Marcaccio, M.; Bossi, A.; Prodi, L.; Paolucci, F. *ChemElectroChem* **2017**, *4*, 1690−1696.
(38) Hsu, C.-W.; Longhi, E.; Sinn, S.; Hawes, C. S.; Young, D. C.; Kruger, P. E.; Cola, L. D. *Chem. - Asian J.* **2017**, *12*, 1649−1658.
(39) Kanoufi, F.; Zu, Y. B.; Bard, A. J. *J. Phys. Chem. B* **2001**, *105*, 210−216.
(40) Miao, W.; Choi, J.-P.; Bard, A. J. *J. Am. Chem. Soc.* **2002**, *124*, 14478−14485.
(41) Stringer, B. D.; Quan, L. M.; Barnard, P. J.; Wilson, D. J. D.; Hogan, C. F. *Organometallics* **2014**, *33*, 4860−4872.
(42) Hesari, M.; Workentin, M. S.; Ding, Z. *ACS Nano* **2014**, *8*, 8543−8553.
(43) Wang, F.; Lin, T.; Zhao, T.; Hu, D.; Wu, T.; Liu, Y. *J. Am. Chem. Soc.* **2016**, *138*, 7718−7724.
(44) Li, X.; Zhang, H.; Tang, Y.; Wu, P.; Xu, S.; Zhang, X. *ACS Sens.* **2017**, *2*, 810−816.
(45) Yin, C.; Wu, Y.; Li, X.; Niu, J.; Lei, J.; Ding, X.; Xiao, D.; Zhou, C. *Anal. Chem.* **2018**, *90*, 7371−7376.

https://dx.doi.org/10.1021/acs.analchem.0c04284
Anal. Chem. 2021, 93, 1686−1692